International Journal of Extreme Manufacturing

Femtosecond laser additive and subtractive micro-processing: enabling a high-channel-density silica interposer for multicore fibre to silicon-photonic packaging

OPEN ACCESS
IOP Publishing | IMMT
International Journal of Extreme Manufacturing
Int. J. Extrem. Manuf. 1 (2019) 045002 (9pp)
https://doi.org/10.1088/2631-7990/ab4d51

Femtosecond laser additive and subtractive micro-processing: enabling a high-channel-density silica interposer for multicore fibre to silicon-photonic packaging

Gligor Djogo[1], Jianzhao Li[1], Stephen Ho[1], Moez Haque[1], Erden Ertorer[1], Jun Liu[2], Xiaolu Song[2], Jing Suo[2] and Peter R Herman[1]

[1] The Edward S Rogers Sr Department of Electrical & Computer Engineering, University of Toronto, Toronto, Canada
[2] Transmission & Access Research Department, Huawei Technologies Co., Ltd, Dongguan, People's Republic of China

E-mail: g.djogo@mail.utoronto.ca

Received 28 August 2019, revised 25 September 2019
Accepted for publication 13 October 2019
Published 6 November 2019

Abstract

Great strides have been made over the past decade to establish femtosecond lasers in advanced manufacturing systems for enabling new forms of non-contact processing of transparent materials. Research advances have shown that a myriad of additive and subtractive techniques is now possible for flexible 2D and 3D structuring of such materials with micro- and nano-scale precision. In this paper, these techniques have been refined and scaled up to demonstrate the potential for 3D writing of high-density optical packaging components, specifically addressing the major bottleneck for efficiently connecting optical fibres to silicon photonic (SiP) processors for use in telecom and data centres. An 84-channel fused silica interposer was introduced for high-density edge coupling of multicore fibres (MCFs) to a SiP chip. Femtosecond laser irradiation followed by chemical etching was further harnessed to open alignment sockets, permitting rapid assembly with precise locking of MCF positions for efficient coupling to laser written optical waveguides in the interposer. A 3D waveguide fanout design provided an attractive balancing of low losses, mode-matching, high channel density, compact footprint, and low crosstalk. The 3D additive and subtractive processes thus demonstrated the potential for higher scale integration and rapid photonic assembly and packaging of micro-optic components for telecom interconnects, with possible broader applications in integrated biophotonic chips or micro-displays.

Keywords: femtosecond laser micro-processing, photonic packaging, waveguide fanout, fibre socket, multicore fibre, space-division multiplexing, silicon photonics interposer

(Some figures may appear in colour only in the online journal)

1. Introduction

Over the past three decades, ultrafast lasers have emerged as a robust and reliable tool, building on their novel material interaction physics to enable remarkable advancements in research as well as in medical and industrial applications [1–5]. The accumulated understanding of multi-photon non-linear interactions has further opened the domain for laser processing inside of optically transparent materials (polymers, glasses, semiconductors, and ceramics) to induce highly localized heating and nano-structuring effects that include micro-explosion of near-spherical, filament, or planar cavities

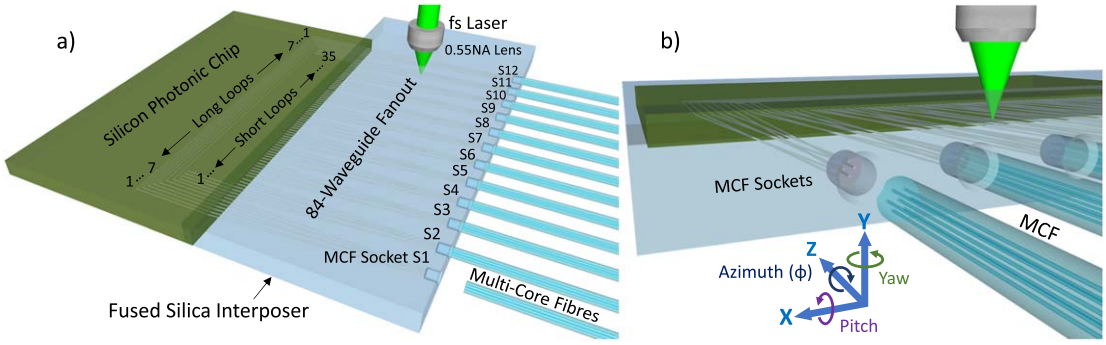

Figure 1. Schematic of the edge coupling interposer, providing a compact packaging solution for interconnecting 84 channels between 12 multicore fibres (MCFs) to silicon photonic (SiP) optical processing chip. (a) A femtosecond (fs) laser inscribes an optical waveguide fanout together with etching-tracks that open into MCF alignment sockets after chemical etching. The additive and subtractive laser processing of silica facilitates submicron self-alignment of MCFs to efficiently couple with the interposer waveguides, (b) dramatically reducing the complexity of fibre alignment and packaging from 5-axis to single-axis (azimuthal) alignment.

through to gentle changes in refractive index and volume nanograting formation [6–10]. These processes have contributed to rapid advances in the miniaturization and integration of photonic, micro-mechanical, and biomedical devices into compact packaging systems with new flexible geometries. Today, buried optical waveguides and circuits [9, 11–13], volume diffractive optical elements [14, 15], opto-fluidics and micro-fluidics [16–19], optical data storage [20, 21], and multi-functional lab-in-fibre [22] can be fabricated in flexible three-dimensional (3D) arrangements inside of transparent materials, constituting new modes of 3D additive and subtractive micro- and nano-processing [23].

On the basis of these novel capabilities, ultrafast lasers are finding niche opportunities in advancing today's high-volume manufacturing towards new 3D geometries, while continuously shrinking device footprint, increasing packaging density, and improving functional integration [24]. One exceptional opportunity lies in the area of photonic packaging, targeting optical communication and data centres. Here, relentless demands for faster and higher capacity networks are being driven on the paradigms of the 'Internet of Information' and the 'Internet of Things'.

In this direction, the well-developed silicon photonics (SiP) platform—with high-density signal processing capability and CMOS manufacturing compatibility—is now poised to enter optical communication and data centre markets [25]. However, bottlenecks remain in the interfacing of the high-density SiP circuits with traditional single-mode fibres (SMFs) due to the large fibre diameter (125 μm). This is driving the development of space-division multiplexing (SDM) [26, 27], such as multicore fibres (MCFs) [28, 29], few-mode fibres [30], and hybrids of both [31], rather than shrinking the fibre diameter and facing mechanical limits. Accordingly, the fibre-to-SiP-chip packaging faces demanding challenges today due to the 3D routing geometries required for both linear edge and out-of-plane grating coupling [32–34] to meet low-loss, low-crosstalk, and high-density packaging with a process scalable to high-volume production.

Pitch reducing optical fibre arrays [35] have shown promise in SDM for fibre-to-SiP-chip interfacing but may not scale up channel number and provide the flexibility as demonstrated to date with 3D glass fanouts [36–38]. Glass fanouts rely on ultrafast laser direct writing [9, 12] of 3D waveguides to interface SMF and MCF arrays by both (1D) edge or (2D) grating coupling to the SiP chip. Such glass interposers manifest various benefits including flexible 3D designs, compact and low-profile packaging, capacity for mass production, and adaptability to both grating and edge coupling. However, the fibre-to-glass interposer alignment and packaging remains a highly tedious and time-consuming processing step, requiring numerous successive iterations of multi-axis positioning, index-matched adhesive dispensing, and curing.

In this paper, we combined ultrafast laser internal additive and subtractive processing techniques to showcase an advanced glass interposer design, where a 3D waveguide fanout has been integrated with fibre guiding sockets to dramatically reduce the time for MCF alignment and packaging with a SiP chip. This comprehensive paper builds on our prior report [39] to provide full design, fabrication, and packaging details, along with a full spectral assessment and breakdown of insertion losses. The arrangement in figure 1(a) presents an 84-channel interposer for edge coupling of twelve MCFs to a SiP chip. The fibre alignment sockets (figure 1(b)) were formed with the technique of femtosecond laser irradiation followed by chemical etching (FLICE) [16–19] to precisely match the fibre diameter and secure fanout waveguide positions to register with the seven guiding cores in each MCF. In this way, the complexity of MCF-to-interposer packaging was considerably reduced from 5-axis alignment to only single axis (azimuthal) alignment. The interposer demonstrates the potential for high-density optical input/output packaging systems with low insertion loss and channel crosstalk. The socket-based fibre packaging reduces the demand on alignment and the number of assembly components, promising more functional and lower cost optical systems in optical communication and data centres, as well as more broadly in biophotonics and heads-up displays.

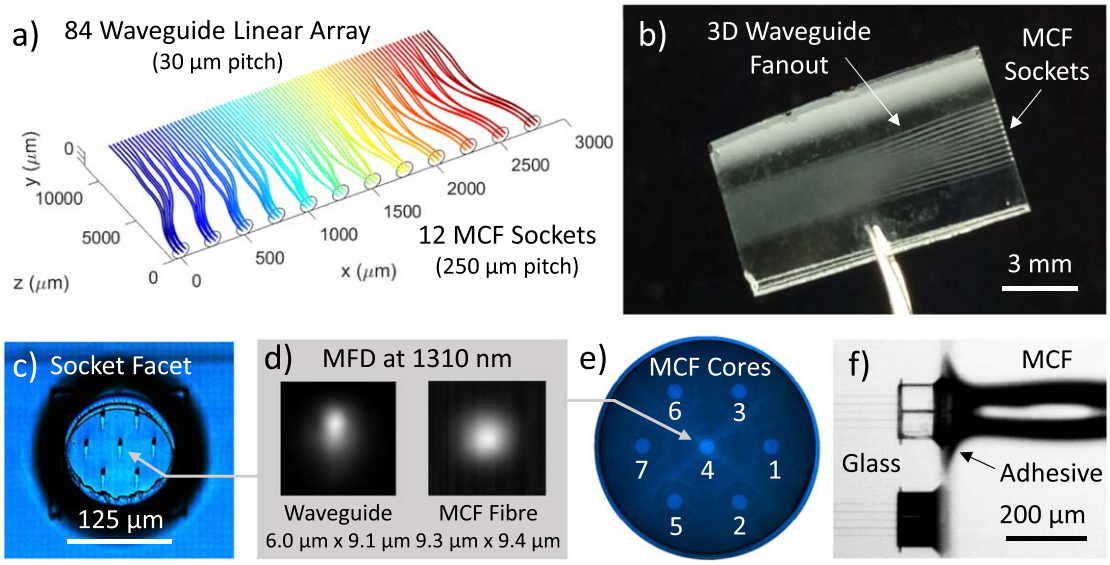

Figure 2. (a) Schematic for the waveguide routing design, fanning out from a linear array (SiP chip at back) to 12 socket positions for MCF packaging. (b) Photo of the fabricated fused silica interposer. (c) End view of a MCF socket, showing precisely positioned waveguides on the buried facet. (d) Mode field images and diameters of an interposer waveguide in comparison with a MCF core for 1310 nm. (e) Image of a cleaved MCF facet showing hexagonal arrangement of the seven core waveguides and their labels. (f) Side-view image of MCF after packaging into the interposer alignment socket with UV cured adhesive. Buried waveguides are visible in the interposer that align with MCF cores.

2. Methods: laser micro-processing and photonic packaging

Laser micro-processing of fused silica interposers was optimized to produce low loss optical waveguides and fibre alignment sockets to assist with the assembly, alignment, and packaging to MCFs and a SiP chip. An optimized design of the interposer, limited by facet coupling, propagation, and bending losses along with crosstalk, is first described to meet the objective for low insertion loss packaging. Laser fabrication of the interposer is then presented and followed with the optical characterization and packaging procedures.

2.1. Interposer design objective

The interposer schematic in figure 1(a) shows 84 waveguides fanning out from a densely packed linear array on 30 μm pitch at the SiP chip side into a 2D grid pattern matching with the seven core positions of each MCF, laid out over twelve sockets. The SiP chip provided return channels in 42 loops, divided into seven long loops that connected sockets labelled S1 and S12, and 35 short loops that connected adjacent channels distributed over sockets S2–S11 (figure 1(a)). Each silicon waveguide channel terminated at the facet with an air-suspended cantilever inverse taper to serve as a mode expander for better matching with the interposer waveguide mode size. The waveguides only guided a single polarization and the positional accuracy of channels was negligible.

On the opposing facet of the interposer, the MCF alignment sockets were arranged in a linear array on 250 μm pitch, centred at ~100 μm depth below the top surface, thus providing ample alignment and adhesive dispensing space for the 125 μm diameter fibre as seen in figure 1(b). The final package was evaluated for light transmission in the 1260–1680 nm telecom band, focusing on 1310 and 1550 nm principal wavelengths.

2.2. Waveguide fanout layout

The final design for the 3D layout of the 84 waveguides in the interposer is shown in figure 2(a). The channel density decreased from 33.3 channels per mm on the SiP chip facet to ~30 channels per mm on the MCF facet. Individual waveguides followed a sequence of straight and circular arc bends, optimized for minimum path length difference and low bending loss, while avoiding close proximity to minimize crosstalk. A minimum bend radius of 60 mm was selected for low insertion loss, making a minimum fanout length of 11.9 mm necessary to accommodate a ~300 μm offset (X-axis) for connecting the outermost MCFs to the long loop channels in the SiP chip. The closest 3D separation between any two waveguides was about 28 μm, sufficient to avoid crosstalk. The optical path length difference over all channels was actively tuned to a maximum of 28 μm by inserting additional pathlength arcs in the shorter path, centremost, waveguide tracks.

Multiple waveguide fanouts were laser patterned inside of a single silica wafer and later separated by diamond cutting or more precisely by laser filament scribing [40], offering reliable and reproducible fabrication of interposers. This 3D laser processing yielded a silica interposer footprint of 10 mm by 12.7 mm as shown in figure 2(b).

2.3. Additive laser micro-processing: waveguides

The interposer required both additive and subtractive fabrication techniques that were applied in two consecutive steps.

The fused silica wafer was first laser irradiated to inscribe waveguide and nanograting tracks and then wet etched in 5% hydrofluoric acid (i.e. FLICE) to selectively open the nanograting tracks [16–19] forming the alignment sockets.

The femtosecond laser inscription was carried out with an integrated computer-controlled system of laser and beam controls with precision positioning stages. A fibre laser based on chirped-pulse-amplification and second harmonic generation (Amplitude Systèmes Satsuma HP^2) provided 515 nm wavelength light with a pulse duration of 250 fs and beam quality M^2 of around 1.1. The laser exposure was applied at a repetition rate of 500 kHz and focused through a 0.55 numerical aperture (NA) aspherical lens (Newport 5722-A-H), filling ~40% of the lens aperture. Nano-positioning stages (Aerotech PlanarDL-200XY and ANT130-110-L-Z) translated the laser focal interaction with respect to the 3D volume of the wafer with submicron accuracy and 100 nm repeatability.

The laser exposure for writing of waveguides in a single scan was optimized for mode-size matching and minimum propagation loss by manipulating laser pulse energy, scanning speed, and repetition rate.

2.4. Subtractive laser micro-processing: MCF sockets

The MCF socket design was targeting a snug sliding guidance of the fibre to a sufficient depth to firmly lock the MCF into the desired *XYZ*, pitch, and yaw positions (figure 1(b)). The FLICE method was optimized to open the alignment sockets to dimensions with submicron precision, while reducing laser writing time, minimizing induced stresses, and creating smooth surfaces to mate with the fibre facet. Overlapping scans of nanograting tracks were traced around the circumference of the cylindrical socket shape, and then along the back plane, to provide optically flat etched surfaces for efficient mode coupling (figure 2(c)). Laser inscription of waveguides was completed in the same step to accurately register positions to the 37 μm pitch MCF cores (figure 2(e)). However, a vertical displacement of the waveguide mode position relative to the cylindrical etched socket hole required an additional (*Y*-axis) offset to be tuned into the laser procedure to minimize the *Y*-axis mode-alignment loss between fanout waveguides and MCF cores.

2.5. Interposer photonic packaging

The insertion losses of the interposer waveguides were assessed and optimized independently of the SiP or MCF packaging to ensure that low overall insertion loss was obtainable on all 84 channels at 1310 and 1550 nm wavelengths. The incremental losses of MCF socket packaging and then SiP edge coupling were separately characterized on key channels and further broadened to all channel testing by following an iterative alignment procedure.

Insertion losses were measured with an optical spectrum analyser (Ando AQ6317B) using a broadband unpolarized light source (Agilent 83437A) covering 1260–1680 nm wavelengths. The characterization process followed standard fibre butt-coupling methods [41], using nano-positioning stages (Luminos Cor/Align P3, P5, and P6) for fibre-to-facet alignment to record the lowest loss spectra. Losses were assessed with respect to direct fibre-to-fibre coupling with index matched liquids (Cargille Labs Refractive Index Liquid) applied at the relevant interfaces. The interposer was probed by both standard SMF (Corning SMF28) and MCF (Chiral Photonics MCF-007_2). The MCF was part of an all-fibre fanout (Chiral Photonics MCFFO-P-07/37-1550-SM01-FC/APC-60) such that all seven MCF cores could be accessed by individual SMFs. Index matched liquid was not applied to the sockets at this stage, adding Fresnel reflection loss.

For profiling of the interposer waveguide mode (figure 2(d)), a tuneable laser (Photonetics TUNICS-BT, Keysight 81600B) at a fixed wavelength was launched into the waveguides and magnified images of the output facets were recorded with a beam profiling camera (Spiricon LBA-FW-SCOR20, Xenics XEVA-7080).

The MCF-to-socket alignment was visually assisted by launching red laser light (Thorlabs S1FC635) into select MCF cores while monitoring light scattering from the interposer waveguides. The MCF was then azimuthally aligned for the lowest average loss on all seven core channels at the principal wavelength. Optical adhesive (Norland NOA 61) was dispensed and UV cured in steps to fix the MCFs one at a time to each of the twelve sockets (figure 2(f)).

For edge coupling to the SiP chip, the interposer and MCF package was separately mounted on a nano-positioning stage (Luminos Cor/Align P6) and guided to the SiP chip with two viewing cameras, using all 6 axes' positioners. Insertion losses were minimized first on short loops, and then on long loops, prior to final bonding with index matched adhesives. Several approaches for the SiP chip-to-interposer alignment and bonding were examined, divided mainly into completing edge-to-edge bonding (Norland NOA 136 adhesive) prior to substrate bonding (Norland NOA 61 adhesive) or by reversing the procedure. For the latter, customized silica spacers were fabricated to vertically match the interposer waveguide positions with the cantilevered waveguide tapers on the SiP chip. The final package, including bonding to a ceramic substrate, is shown in figure 3, with SiP loops enlarged.

3. Results: interposer assessment

The optimization of waveguide fanouts and MCF alignment sockets are presented separately for the interposer, followed with assessment of the MCF and SiP chip packaging into a complete photonic system.

3.1. Waveguide optimization

The laser exposures were based on prior studies of writing waveguides with femtosecond laser focusing in fused silica, around 100 μm deep under the surface, where slow writing speeds of 0.05–0.2 mm s^{-1} were found to be optimal [41, 42].

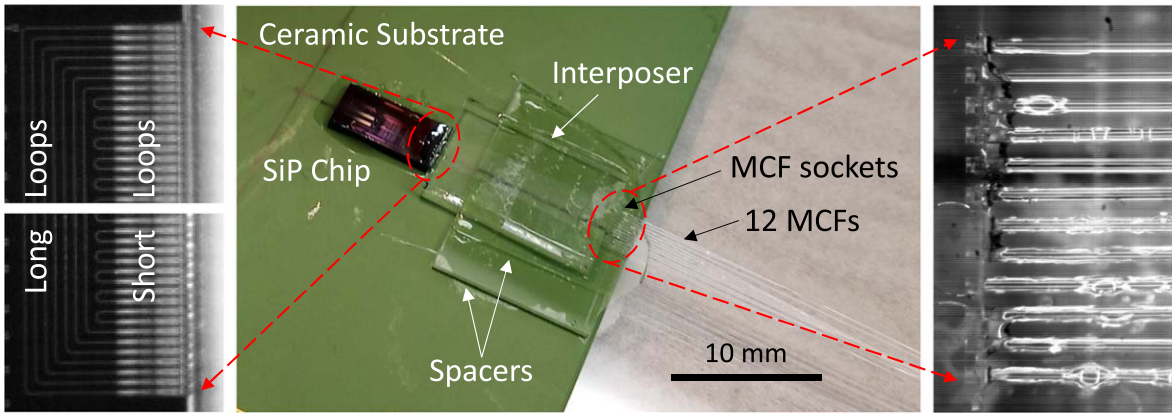

Figure 3. Optical image of a fully packaged interposer (centre) bonded with 12 MCFs (right) and edge coupled with a SiP chip (left). The enlarged view of the SiP chip shows the short and long loops for testing insertion loss.

Selecting a 0.1 mm s^{-1} scanning speed, insertion loss spectra for straight waveguides of 25.4 mm length were recorded as presented in figure 4(a) for laser pulse energies varying from 92 to 564 nJ. The tilting of the spectra reverses from negative to positive slope, showing that optimal insertion loss shifts to longer wavelengths with increasing pulse energy. However, spectral oscillations in the losses, that were prominent for 320 nJ exposure or weakly evident at shorter wavelengths for 256 nJ exposure, were indicative of multi-mode guiding and were avoided. The insertion loss for the 1310 and 1550 nm wavelengths were replotted in figure 4(b) (left-hand axis). Noting the shaded zone for multi-mode guiding, the data show that a minimum insertion loss for single-mode guiding was obtained for exposures in the 160–204 nJ range.

The transverse (MFD_X) and vertical (MFD_Y) mode field diameters were also influenced by the pulse energy as shown in figure 4(b) (right-hand axis), reaching minimum values of 6.0 by 9.1 μm, respectively, at 1310 nm wavelength, and 9.1 by 11.1 μm, respectively, at 1550 nm wavelength. These exposures favourably coincided with the exposure for minimum insertion loss. The minimum mode size for 1310 nm lays between the smaller 6.1 μm mode diameter of the cantilevered waveguide taper at the SiP facet and the larger 9.3 μm by 9.4 μm diameters of the MCF mode as shown in figure 2(d). Thus, mode-mismatch losses were not significant without the need for tapering of laser written waveguides [43].

The 160 nJ pulse energy condition was selected as the optimal laser writing exposure for obtaining lowest overall insertion loss at both wavelengths. At this exposure, waveguide propagation losses of −0.53 dB cm^{-1} and −0.30 dB cm^{-1} were obtained at 1310 and 1550 nm, respectively, by comparing insertion loss in 25.4 and 12.7 mm long waveguides. In this way, mode-mismatch losses of −0.35 dB per facet and −0.45 dB per facet were inferred at 1310 and 1550 nm wavelengths, respectively, for coupling to SMF.

Waveguide bending losses in both the horizontal and vertical planes were assessed at the optimum pulse exposure through S-bends with fixed 100 μm lateral offsets and different radii. Bending loss became appreciable for a 60 mm radius of curvature as shown in figure 4(b) for each of the principal wavelengths. Vertical bending induced significantly more loss than horizontal bending, for example, generating −1.22 dB and −0.13 dB additional loss, respectively, at the 1310 nm wavelength. The main influence on vertical bending loss may arise from mode radiation into the zone of negative refractive index modification that forms above the guiding zone, as seen in the backlight facet view of the socket (figure 2(c)). Although vertical bending was necessary, the present fanout design (figure 2(a)) relied on significantly larger horizontal bends, with maximum offsets of ∼273 μm (X-axis) compared with ∼63 μm vertically (Y-axis).

3.2. MCF socket optimization

The FLICE subtractive micro-processing was controlled to submicron precision by writing narrow etching tracks with dense line-to-line spacing and by timing the HF acid etching, resulting in smooth and uniform cylinders into which a MCF could slide with a snug fit. The MCF socket depth (100 μm) offered minimal wall tapering and sufficient rigidity to resist bending along pitch and yaw to better than ±1°, without the excessive fabrication time of deeper sockets. The back plane was defined by nanograting tracks written with half-micron pitch, resulting in a mirror-like finish (figure 2(b)) with an estimated roughness of 10 nm rms as previously reported for microchannel walls [44]. The waveguides were also terminated ∼7 μm from the socket back plane and opposing glass facet to present a stop layer to the FLICE etching step.

The centre waveguide position (figure 2(c)) was optimized to meet within ±0.25 μm of the centre MCF core (figure 2(e), core 4) by first testing coupling to a SMF. A socket-to-waveguide offset was applied in 0.5 μm increments to yield a minimum coupling loss when the waveguide was shifted 2.5 μm higher (+Y-axis in figure 1(b)). This offset accounted for a displacement of the waveguide guiding centre from the etch-guiding nanograting volume. No offset improvement could be inferred on similar tuning along the X-axis.

Although all interposer waveguides were written to match the MCF layout, not all of the outer waveguides

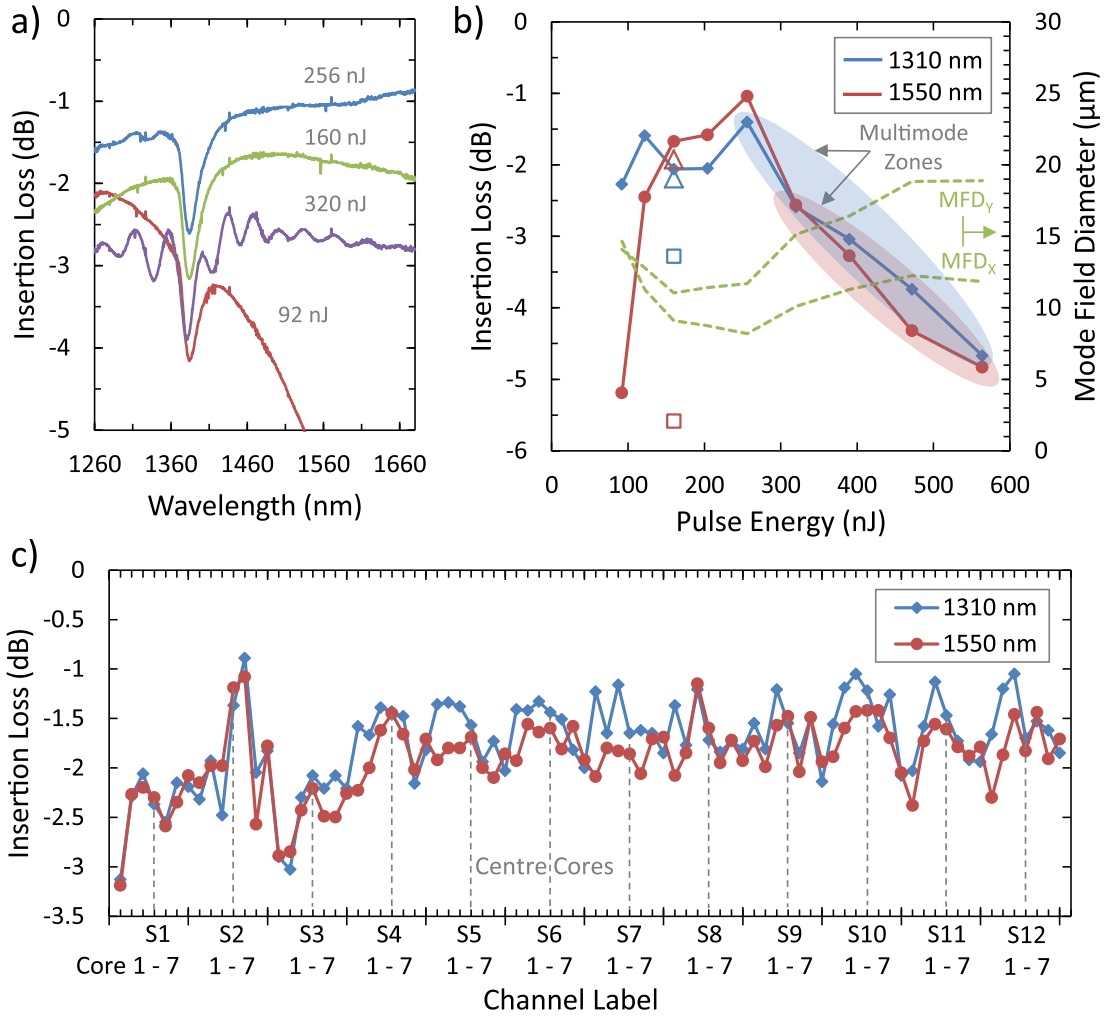

Figure 4. (a) Spectra of insertion loss for 25.4 mm long straight waveguides formed in fused silica at 0.1 mm s^{-1} scanning speed, with ultrafast laser pulses at 515 nm wavelength and 250 fs duration, for varying laser pulse energies. (b) Optimization of insertion loss through straight waveguides (25.4 mm length) for 1310 and 1550 nm guiding, with increasing laser pulse energy. Insertion losses reach minima at the onset of multimode guiding (shaded zones). S-bend waveguide losses at 160 nJ exposure and 60 mm radius of curvature are indicated with triangle (△) and square (□) markers, for horizontal and vertical bends, respectively. Mode field diameters for straight waveguides at 1550 nm (dashed lines/right-side axis) reach minima in the same exposure range for minimum waveguide loss. (c) Single-pass insertion loss across 84 interposer channels, probed with respect to SMF-MCF centre core coupling. Centre waveguides in each socket (core 4) are indicated by vertical dashed lines. The MCF-to-socket coupling was in air.

(figure 2(e), cores 1-3, 5-7) could reach the minimum loss simultaneously under azimuthal alignment. The insertion loss followed a repeatable pattern on 60° rotations of the MCF, but with minimum loss angles differing by up to 2° on the azimuth. This angle difference translates to ∼1 μm of lateral misalignment of the waveguides to MCF cores, on which one expects ∼0.2 dB mode-alignment loss. However, the insertion loss for the centre channel remained unchanged during these rotations, thus pointing to highly concentric alignment of the core fibre to the cladding surface during manufacturing. Radial positional errors in the MCF cores could not be inferred during the MCF rotational alignment, but similar errors of ∼1 μm are consistent with optical microscopy imaging of the MCF at the limit of resolution. The coupling loss variances also shifted when using MCF from different parts of the spool. Hence, such losses could not be readily compensated by adjusting the interposer waveguide layout. Further improvements in the MCF manufacturing would improve the present packaging loss.

Nevertheless, the MCF-to-interposer losses under socket guidance could be optimized to 0.2 dB on individual channels, which was not far from the losses obtained by direct butt-coupling to a similar interposer without socket terminations. Hence, alignment sockets posed no additional cost on the insertion loss budget for fibre coupling to 3D optical circuits.

3.3. Silica interposer characterization

The losses across 84 channels for the silica interposer are shown in figure 4(c), updated from a prior report [39], having an average loss of −1.7 dB at 1310 nm and −1.9 dB at

1550 nm wavelengths. The contributions to total loss included a small socket loss (<0.2 dB), a mode-mismatch loss between the interposer and SMF waveguides (~0.7 dB), and waveguide propagation and bending loss (1.0 dB on average) over a 12.7 mm length.

Figure 4(c) reveals a periodic pattern of channel loss (~1 dB range) over seven channels, or once every socket. This pattern is attributed to variations in coupling loss between the outer MCF cores and interposer waveguides, as described in the MCF socket optimization section above. The centre core 4 losses indicated in figure 4(c) show low variance from socket-to-socket as they were less susceptible to azimuthal misalignment during the MCF probing. The data were also influenced by a non-trackable, but periodic ~0.3 dB variation in insertion loss over the seven cores of the all-fibre MCF-to-SMF fanout.

3.4. Interposer packaging losses

The MCF packaging was greatly facilitated by the alignment sockets, as individual fibres were sequentially inserted, rotated for optimized loss, and locked in place by dispensing and UV light curing of optical adhesive. A single MCF is shown bonded inside of an interposer socket in figure 2(f), while the full array of twelve MCFs is shown bonded on the right side of the interposer in figure 3. The index-matched adhesive improved the insertion loss by an average of 0.3 dB after curing, reducing Fresnel reflection loss as compared to the losses of figure 4(c). After curing, insertion losses remained stable for multiple days and without showing degradation due to exposure at the relatively modest infrared light probing intensities used here, as is typically applied in telecom systems. Overall, the MCF-to-socket guidance demonstrated a highly promising concept for rapid SDM auto-alignment and packaging, offering submicron registration of MCF cores to fanout waveguides across 84 densely packaged channels.

In the final step of packaging with the SiP chip, single-pass loop losses through the interposer were calculated by subtracting the average loss of the all-fibre MCF fanout (1.3 dB per pass) and the polarization filtering loss of the unpolarized source through the polarizing SiP chip waveguides (3 dB) from the measured full-loop insertion loss, and then dividing the remainder into two passes. The opportunity for low-loss packaging was evident during the dry alignment, with low single-pass losses being routinely recorded, for example, −4.9 dB on short loop 1 and −5.7 dB on long loop 7, as plotted in figure 5(a) (interposer chip 1).

However, the bonding of the interposer to the SiP chip proved to be demanding. Direct edge-to-edge bonding as a first step was not a promising approach, since dispensing of adhesive did not improve mode-mismatch losses between the chips as expected. UV curing further imposed lateral and torqueing forces that misaligned the chips, resulting in significantly higher insertion loss across all channels.

The packaging procedure that yielded the lowest loss photonic system was obtained by independently bonding the interposer and SiP chip to the ceramic substrate. Custom-cut silica spacers were positioned under the interposer to closely match waveguide heights (within 20 μm) as shown in figure 3. The interposer was actively aligned for best coupling in air against a SiP chip, which was first bonded to the ceramic substrate. A single-pass loss of −6.6 dB was measured on long loop 1, as indicated in figure 5(a) (chip 2). This loss was recovered to within ~0.1 dB after dispensing adhesive between the spacer plates and the interposer. However, shrinkage of the adhesive during UV curing offset the vertical alignment by ~2 μm, thus increasing the single-pass losses to −8.4 and −7.2 dB for 1310 and 1550 nm, respectively. Attempts to dispense and cure other adhesives with different viscosities and values of refractive index between the interposer-SiP facets resulted in higher losses, possibly owing to optical and mechanical distortion of the air-suspended tapered silicon waveguides under adhesive flow.

The single-pass losses through all SiP loop channels are summarized in figure 5(a), updated from a prior report [39], for the fully packaged photonic system, where adhesive was applied at the interposer-to-SiP-chip interface as a final packaging step. The losses for the long and short loops were similar, ranging from −6.9 to −10.9 dB (−8.0 dB average) at 1310 nm, and from −5.5 dB to −8.2 dB (−6.5 dB average) at 1550 nm. The reported values consisted of the interposer loss shown in figure 4(c) (1.7–1.9 dB), mode-mismatch loss at the SiP chip (~0.7 dB), and Fresnel reflection loss at the silicon-adhesive-glass interfaces (~0.8 dB), leaving a remaining 1.5 to 2.25 dB packaging loss between the interposer and SiP facet due to alignment and other errors. The propagation and bending losses were negligible in the SiP chip waveguide loops. Channel crosstalk was better than −20 dB, limited by the noise floor of the OSA.

Full-loop insertion losses across the full telecom spectrum are presented in figure 5(b) showing the best (short loop 17) and the worst (short loop 2) cases as well as the average losses for each of the long and short loop groups. These spectra include the 3 dB polarization filtering loss and the 2.6 dB double-pass loss through the all-fibre MCF fanout. The best transmission was observed around 1560 nm although the overall design was optimized for 1310 nm. This wavelength change arose due the vertical displacement of the interposer during the UV curing of the silica spacers, shifting the alignment to a position favouring 1560 nm guiding between the laser written waveguide and the SiP channel taper.

4. Discussion

The flexibility of 3D femtosecond laser micro-processing enabled both additive and subtractive fabrication of a novel optical interposer, integrating low-loss waveguide fanouts with high-precision registration to MCF alignment sockets. In this way, low-loss optical interconnects provided 84 input/output channels between multicore optical fibre and high-density silicon photonics circuits. The fused silica interposer presented a low footprint of 10 mm by 12.7 mm.

The packaging challenge of MCF to silica wafer was addressed by introducing alignment sockets made by FLICE. These finely tuned holes lend themselves to mass manufacturing

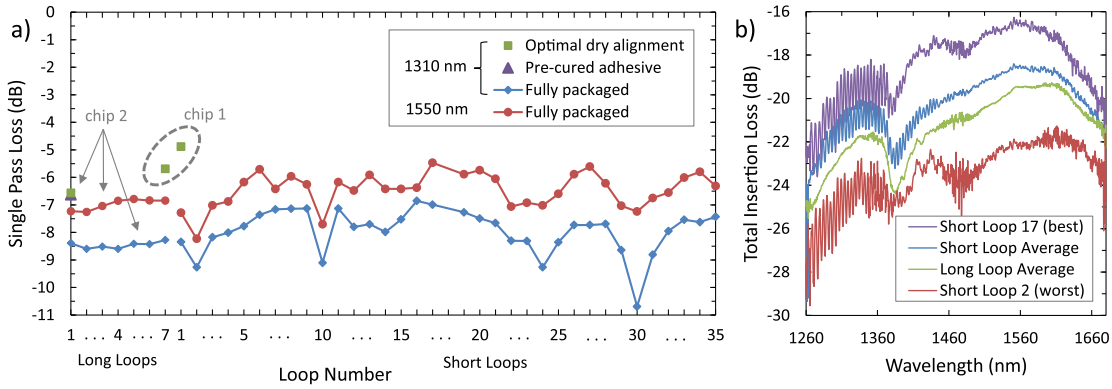

Figure 5. (a) Single-pass insertion loss at 1310 (blue) and 1550 nm (red) wavelengths, probed by 12 MCFs through the interposer and returned through the SiP short and long loop channels. Losses for select loops are presented prior to dispensing (dry) and curing (pre-cured) of adhesive for the final interposer-to-SiP-chip packaging step. (b) Spectra of total (full pass) insertion loss for the fully packaged photonic system (chip 2), presenting best and worst packaged loops, as well as the average loss for short and long loops, respectively. Losses include 3 dB polarization filtering loss and 2.6 dB for double passes in the all-fibre MCF fanout used for probing each channel.

by greatly reducing alignment complexity and fibre packaging time without adding any insertion loss.

The interposer could be improved using a more compact fanout design of 7.1 mm in length by reducing the socket pitch to 210 μm to match the SiP waveguide pitch. This further reduces the maximum horizontal offset of the fanout to 53 μm (X-axis), promising a 0.3 dB cut in propagation and bending loss. Nevertheless, the current interposer design was found to meet the low-loss requirement (figure 4(c)) for packaging to the MCFs.

The packaging of the interposer to SiP chip was the most challenging step and could be improved by a procedure to vertically displace the interposer (i.e. $\sim$2 μm) to counteract the adhesive curing shrinkage. However, our attempts showed mixed results in under- or over-compensating due to differences in the interposer-to-spacer distance with each trial. Alternatively, the precision of FLICE processing may permit formation of a customized alignment edge on the interposer to register pitch, yaw, roll and vertical positioning to the SiP chip.

Further improvements of up to 1 dB to reduce mode-mismatch losses may be possible by laser writing of tapered waveguides [43] in the interposer to better match the SiP waveguide and MCF modes. By employing one or more of these strategies, one should find that single-pass losses of better than −5 dB could be routinely obtained for interposer packaging, matching with the best insertion loss as reported for the dry alignment case (figure 5(a), chip 1).

5. Conclusion

Additive and subtractive laser processing of a 3D optical interposer for SDM was introduced for the interconnection of MCF with a SiP chip, yielding average single-pass channel losses of −8.0 dB and −6.5 dB for 1310 nm and 1550 nm wavelengths, respectively. Fibre alignment sockets presented a dramatic simplification of the MCF alignment and packaging, reducing 5-axis alignment to a single azimuthal alignment step. Moreover, the interposer socket significantly strengthened and stabilized the fibre bonding over direct facet bonding.

A key opportunity lies in further improvement in the final bonding step for edge coupling to the SiP chip, where losses of better than −5 dB per pass may become routinely possible. Adoption of waveguide tapers [43] can further improve mode-mismatch loss. Development of faster laser writing processes is also desirable to speed up fabrication times from hours to minutes per device, and open prospects for mass production.

More broadly, the 3D additive and subtractive micro-processing of glass has successfully demonstrated new directions for fabricating and assembling micro-optic components into compact photonic systems. The submicron control of socket sizes and their integration with waveguides could further benefit photonic packaging of micro-lasers, nonlinear components, or complex fibre assemblies. Thus, the opportunity that femtosecond lasers have found in optical communications could be expanded to biophotonic chips or micro-display systems.

Acknowledgments

Financial support from Huawei Technologies Co., Ltd, China (Project YB2016020025) is gratefully acknowledged.

ORCID iDs

Gligor Djogo https://orcid.org/0000-0001-5396-969X

References

[1] Sugioka K and Cheng Y 2014 *Light Sci. Appl.* **3** e149
[2] Phillips K C, Gandhi H H, Mazur E and Sundaram S K 2015 *Adv. Opt. Photon.* **7** 684
[3] Malinauskas M, Žukauskas A, Hasegawa S, Hayasaki Y, Mizeikis V, Buividas R and Juodkazis S 2016 *Light Sci. Appl.* **5** e16133

[4] Braun M, Gilch P and Zinth W 2007 *Ultrashort Laser Pulse in Biology and Medicine* (New York: Springer)
[5] Lubatschowski H, Heisterkamp A, Will F, Singh A I, Serbin J, Ostendorf A, Kermani O, Heermann R, Welling H and Ertmer W 2003 *RIKEN Rev.* **50** 113
[6] Schaffer C B, Glezer E N, Nishimura N and Mazur E 1998 *Proc. SPIE* **3269** 36
[7] Ashkenasi D, Varel H, Rosenfeld A, Henz S, Herrmann J and Cambell E E B 1998 *Appl. Phys. Lett.* **72** 1442
[8] Kumar K, Lee K K C, Li J, Nogami J, Kherani N P and Herman P R 2014 *Light: Sci. Appl.* **3** e157
[9] Davis K M, Miura K, Sugimoto N and Hirao K 1996 *Opt. Lett.* **21** 1729
[10] Shimotsuma Y, Kazansky P G, Qiu J and Hirao K 2003 *Phys. Rev. Lett.* **91** 247405
[11] Schaffer C B, Brodeur A, Garcia J F and Mazur E 2001 *Opt. Lett.* **26** 93
[12] Nolte S, Will M, Burghoff J and Tuennermann A 2003 *Appl. Phys.* A **77** 109
[13] Ams M, Marshall G D, Spence D J and Withford M J 2005 *Opt. Express* **13** 5676
[14] Itoh K, Watanabe W, Nolte S and Schaffer C B 2006 *MRS Bull.* **31** 620
[15] Gerke T D and Piestun R 2010 *Nat. Photon.* **4** 188
[16] Marcinkevičius A, Juodkazis S, Watanabe M, Miwa M, Matsuo S, Misawa H and Nishii J 2001 *Opt. Lett.* **26** 277
[17] Osellame R, Hoekstra H J W M, Cerullo G and Pollnau M 2011 *Laser Photonics Rev.* **5** 442
[18] Hnatovsky C, Taylor R S, Simova E, Bhardwaj V R, Rayner D M and Corkum P B 2005 *Opt. Lett.* **30** 1867
[19] Sugioka K and Cheng Y 2012 *Lab Chip* **12** 3576
[20] Glezer E N, Milosavljevic M, Huang L, Finlay R J, Her T-H, Callan J P and Mazur E 1996 *Opt. Lett.* **21** 2023
[21] Zhang J, Čerkauskaite A, Drevinskas R, Patel A, Beresna M and Kazansky P G 2016 *Proc. SPIE* **9736** 97360U
[22] Haque M, Lee K K C, Ho S, Fernandes L A and Herman P R 2014 *Lab Chip* **14** 3817
[23] Sugioka K 2019 *Int. J. Extrem. Manuf.* **1** 012003
[24] Jonušauskas L, Mackevičiūtė D, Kontenis G and Purlys V 2019 *Adv. Opt. Technol.* **8** 241
[25] Thomson D *et al* 2016 *J. Opt.* **18** 073003
[26] Klaus W, Puttnam B J, Luis R S, Sakaguchi J, Mendinueta J-M D, Awaji Y and Wada N 2017 *J. Opt. Commun. Netw.* **9** C1
[27] Li G, Bai N, Zhao N and Xia C 2014 *Adv. Opt. Photonics* **6** 413
[28] Saitoh K and Matsuo S 2016 *J. Lightwave Technol.* **34** 55
[29] Hayashi T, Taru T, Shimakawa O, Sasaki T and Sasaoka E 2011 *Opt. Express* **19** 16576
[30] Ryf R *et al* 2012 *J. Lightwave Technol.* **30** 521
[31] Riesen N, Gross S, Love J D, Sasaki Y and Withford M J 2017 *Sci. Rep.* **7** 6971
[32] Kopp V I, Park J, Wlodawski M, Hubner E, Singer J, Neugroschl D, Genack A Z, Dumon P, Campenhout J V and Absil P 2015 *J. Lightwave Technol.* **33** 653
[33] Lee B G *et al* 2010 *Proc. Opt. Fiber Commun. Conf.* PDPA4
[34] Barwicz T *et al* 2018 *Opt. Fiber Technol.* **44** 24
[35] Kopp V I, Park J, Wlodawski M, Singer J, Neugroschl D and Genack A Z 2014 *J. Lightwave Technol.* **32** 605
[36] Thomson R R, Bookey H T, Psaila N D, Fender A, Campbell S, MacPherson W N, Barton J S, Reid D T and Kar A K 2007 *Opt. Express* **15** 11691
[37] Zhao Q, Song X, Dong Z, Gao L, Liu J, Fu S and Zeng L 2016 *IEEE CPMT Symposium Japan (ICSJ)* p 231
[38] Mitchell P, Brown G, Thomson R, Psaila N and Kar A 2014 *Optical Fiber Communication Conf. 2014* M3K.5
[39] Djogo G, Ho S, Haque M, Ertorer E, Li J, Liu J, Song X, Suo J and Herman P R 2019 *Optical Fiber Communication Conf. 2019* Tu2A.7
[40] Li J, Ertorer E and Herman P R 2019 *Opt. Express* **27** 25078
[41] Shah L, Arai A Y, Eaton S M and Herman P R 2005 *Opt. Express* **13** 1999
[42] Eaton S M, Ng M L, Osellame R and Herman P R 2011 *J. Non-Cryst. Solids* **357** 2387
[43] Heilmann R, Greganti C, Gräfe M, Nolte S, Walther P and Szameit A 2018 *Appl. Opt.* **57** 377
[44] Ho S, Herman P R and Aitchison J S 2012 *Appl. Phys.* A **106** 5